CdSe-MoS_2: A Quantum Size-Confined Photocatalyst for Hydrogen Evolution from Water under Visible Light

F. Andrew Frame and Frank E. Osterloh*

Department of Chemistry, University of California, Davis, One Shields Ave, Davis, California 95616

Received: February 10, 2010; Revised Manuscript Received: April 18, 2010

Under visible light irradiation, CdSe-nanoribbons photocatalyze H_2 evolution from aqueous sodium sulfite/sulfide solution with a quantum efficiency of 9.2% at 440 nm, whereas bulk CdSe is not active for the reaction. Photoelectrochemical measurements show that the activity of nano-CdSe is caused by a raised flatband potential (−0.55 V, NHE) which follows from the increased bandgap (2.7 eV) of this quantum confined material. In the presence of a sulfide ion, the flatband potential is fixed to −0.43 V (NHE), slightly below the sulfide redox potential (−0.48 V, NHE). When the nanoribbons are chemically linked to MoS_2 nanoplates that were obtained by exfoliation and ultrasonication of bulk MoS_2, the activity increases almost four times, depending on the mass percentage of MoS_2. Cyclic voltammetry reveals that the enhancement from the MoS_2 nanoplates is due to a reduction of the H_2 evolution overpotential. In contrast, chemical linkage of Pt nanoparticles to the nanoribbons does not affect the photocatalytic activity.

Introduction

The photocatalytic water splitting reaction has received considerable attention as a solar energy driven pathway to hydrogen. Hydrogen is not only an environmentally benign fuel for the generation of power, heat, and electricity, but also a versatile reagent for the synthesis of ammonia and for the conversion of carbon dioxides into methanol and hydrocarbons. Metal chalcogenides[1–9] are promising as catalysts for photocatalytic water *reduction* because their bandgaps allow absorption in the visible region of the spectrum.

Recently, we showed that CdSe nanoribbons are active for photocatalytic H_2 evolution from sulfide or sulfite solution, whereas bulk CdSe is not.[10] We attributed the difference in reactivity to a quantum size effect that increases the bandgap of nano-CdSe (2.7 eV) over that of bulk CdSe (1.7 eV). Here we use data from photoelectrochemistry to confirm that the activation of nano-CdSe is indeed due to the raised flatband potential of the nanocrystals.

We also find that the performance of the nanoribbons can be improved with MoS_2 nanoparticles. Molybdenum disulfide was recently discovered as electrocatalyst for the hydrogen evolution reaction (HER).[11–15] Usually, MoS_2 is prepared by chemical vapor deposition or synthesized from molecular precursors in solution. Here we show for the first time that the chemical exfoliation of bulk MoS_2 leads to MoS_2 nanosheets that are also active for the reaction. On the contrary, platinum nanoparticle-modified CdSe nanoribbons do not exhibit enhanced activity which we attribute to surface poisoning with sulfide and selenide.

Experimental Section

Cadmium chloride was purchased from Baker and Adamson (>99% purity), selenium powder from Aldrich (99.999% purity), hexadecylamine from Acros (>90% purity), trioctylphosphine from Aldrich (technical grade, 90%), octylamine from Acros (>99% purity), carbon monoxide gas from Airgas (chemically pure grade), molybdenum disulfide powder from Acros (98.5% purity), butyllithium in hexanes from Acros, hexane from Fisher Scientific (99.9% purity), hexachloroplatinic acid hexahydrate from Acros (99.90% purity), and sodium citrate dihydrate from Aldrich (>99% purity). Water was purified by a Nanopure II system to a resistivity of >18 MΩ.

CdSe Nanoribbons. The nanoribbons were synthesized according to the published method by Joo et al.[16] The reaction mixture was kept at 70 °C for 24 h, and eight washing cycles were used to remove the selenium starting material. The resulting bright yellow CdSe nanoribbon paste was collected and stored in dark conditions in a sealed flask. Unlike the published method, the CdSe paste was not dried further.

MoS_2 Nanosheets. The nanosheets were made according to the published method by Joensen et al.[17] MoS_2 powder (0.210 g) was added to a 100 mL 2-neck flask under N_2 atmosphere. The flask had 30 mL of 1.6 butyllithium in hexanes added (∼35× molar excess of BuLi) and was stirred for 5 days. The resulting suspension was gravity-filtered under N_2, and the solid washed with ∼100 mL of hexanes and then isolated to a paste. The MoS_2 paste was transferred to a 50 mL round-bottom flask and sealed with a septum. The paste was dried with N_2 to remove volatile hexanes and then quickly quenched with 30 mL of DI water while being sonicated to promote exfoliation. This low-power sonication continued for 30 min. The MoS_2 exfoliated sheets were exposed to high-power ultrasonication for 10 h to reduce sheet size to desired dimensions.

Pt-Citrate Nanoparticles. A solution of a citrate-coated Pt nanoparticles (∼4 nm) was prepared from hexachloroplatinic acid following a published procedure.[18] A flask containing a 30 mL volume of 1% wt aqueous solution of sodium citrate dihydrate was added to a 195 mL aqueous solution containing 0.108 mg of hexachloroplatinic acid. The resulting mixture was brought to reflux for 2 h with stirring. The solution was initially yellow but developed a dark brown color after 30 min of refluxing. The reaction vessel was allowed to cool to room temperature before excess citrate ions were removed from the

* To whom correspondence should be addressed. E-mail: fosterloh@ucdavis.edu.

10.1021/jp101308e © 2010 American Chemical Society
Published on Web 05/24/2010

brown solution by dialysis in 4 L of water using 12 k MWCO dialysis tubing to a conductivity of 1.8 μS/cm over the course of 3 days.

CdSe-MoS_2 Nanocomposites. The assembly was achieved by dispersing small amounts of the synthesized CdSe paste (typically 10−20 mg) in ~25 mL water with minimal sonication. The MoS_2 nanosheets were diluted (if necessary) and sonicated, then added in very small amounts (typically 0.1 to 30% weight relative to CdSe) to the stirred CdSe solution. The CdSe immediately turned slightly yellow-green, and the CdSe-MoS_2 composite solution was stirred for 30 min to achieve total attachment of all the MoS_2. UV−vis analysis of the resulting supernatant confirms that no MoS_2 nanosheets are left in solution.

CdSe-Pt-Citrate Nanocomposites. Assembly was achieved by dispersing small amounts of the synthesized CdSe paste (typically 10−20 mg) in ~25 mL of water with minimal sonication. The Pt sol from dialysis (0.4 mg/L) was diluted in ~10 mL of water. The suspended CdSe ribbons were added to the Pt sol with stirring. The mixture was stirred for further 30 mins, and stored at room temperature for further use. The result was distributed platinum nanoparticles across the CdSe nanoribbons.

Transmission electron microscopy (TEM) measurements were conducted on a Philips CM120 transmission electron microscope operating at 80 keV. Samples for TEM were deposited onto holey carbon-coated Cu grids and washed with ethanol (or chloroform) before drying in an 80 °C oven for one-half hour. UV−vis (ultaviolet−visible) and fluorescence spectra were collected on an Ocean Optics DH2000 light source and HR2000 CG-UVNIR spectrometer and a Yobin Ivon Fluoromax-P fluorometer. Samples were prepared by diluting a small amount of CdSe (or composite) paste in either water or hexadecylamine (HDA)/chloroform solution (~1% wt HDA) as appropriate. Photolysis experiments were carried out using a 300 W Xe arc lamp equipped with a 450 nm long-pass filter and a water IR filter. Inside the 100 mL glass reaction flask the irradiance was measured as 450 mW/cm^2 using a GaAsP detector. For QE measurements, a 440 nm light-emitting diode (LED) array (Roithner Laboratories) was used as an illumination source that produced an irradiance of ~35 mW/cm^2 at the flask. Gas samples were analyzed with a Varian gas chromatograph using Ar carrier gas, a 60/80 Å molecular sieve column, and a thermal conductivity detector. For catalytic measurements about 10 mg of the CdSe-based catalyst were dispersed in 100 mL of 0.1/0.1 M Na_2S:Na_2SO_3 solution and stirred. Oxidation of the sulfide/sulfite system produces thiosulfate, sulfate, and dithionate.[1] Prior to irradiation, the mixture was degassed with five evacuation/Ar backfill cycles and backfilled with Ar to a pressure of ~600 Torr. Samples for gas analysis were periodically removed using the attached gas chromatography system. Electrochemical measurements were performed using a three-electrode cell equipped with a Pt counterelectrode and saturated calomel (SCE) reference electrode. A gold square (1.0 cm^2) served as the working electrode. Films of the semiconductors were fabricated on this electrode by drop-coating and drying in N_2. Electrolytes consisted of either aqueous 1.0 M KCl/20% CH_3OH (pH = 7) or aqueous 0.1/0.1 M Na_2SO_3/Na_2S solution (pH = 9.3). Oxygen was removed from the solutions by degassing with N_2 prior to the measurements. The system was calibrated with the potential of the $K_4[Fe(CN)_6]$ redox couple (+0.36 V vs NHE). Potentials were generated and currents analyzed with a Gamry Reference 600 potentiostat controlled by a personal computer. Photocurrent onset potentials were determined by applying cathodic scans and marking the point when the photocurrent fell below 10% of the highest observed value. Light for photoelectrochemical measurements was produced by a 300 W Xe arc lamp, filtered with a borosilicate glass UV and water IR filter, and directed onto the working electrode using SiO_2 fiber optics. The power at the electrode was 120 ± 20 mW/cm^2 as measured with a GaAsP photodetector.

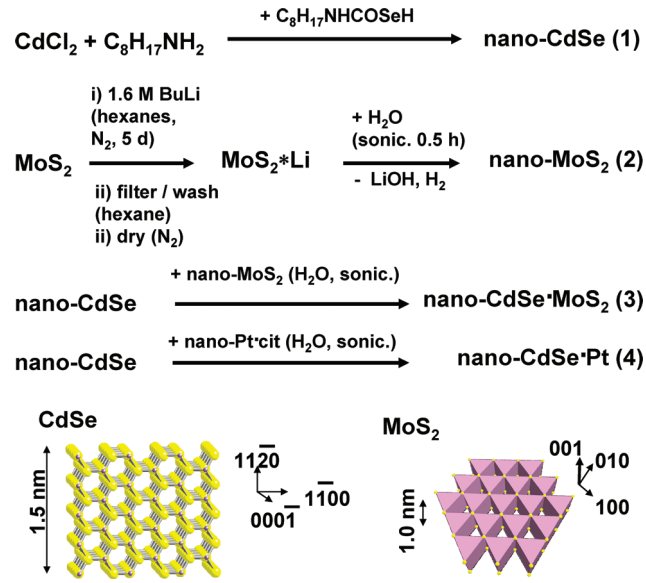

Figure 1. Synthetic scheme for nanocatalysts. Structures for MoS_2 and CdSe were drawn from atomic coordinates.

Results

Materials relevant to this study and their preparation are summarized in Figure 1. CdSe-nanoribbons (**1**) were obtained following the procedure published by Joo et al.[16] Each ribbon consists of 1.5 nm thick wurtzite-type crystal fragments with the orientation shown in Figure 1. These ribbons are coated on their surfaces with octylamine and subsequently assemble into nanowire-like stacks, that can be observed by TEM (Figure 2A,B).

To obtain nano-MoS_2 particles, bulk MoS_2 was exfoliated through intercalation with *n*-butyl lithium, followed by a reaction with water. Initially, this reaction produces MoS_2 crystal fragments of variable sizes (Figure 2C), which can be broken down into smaller particles by ultrasonication. Eventually one obtains sheet-like particles (**2**) with 10 ± 5 nm dimensions, depending on sonication duration and power. As can be seen from the TEM (Figure 2D), the MoS_2 nanoparticles obtained after 12 h of sonication have irregular shapes, but on the basis of the TEM contrast the nanosheet thickness variations are small. According to Jaramillo and co-workers, the active sites for HER are located at the MoS_2 edge sites.[11,14,15] The MoS_2 cocatalysts were attached to the CdSe-nanoribbons according to Figure 1, by stirring mixtures of the components in solution.

TEM reveals that MoS_2 particles readily bind to the nanoribbon surface. Linkage likely involves van der Waals interactions and covalent interactions between the soft selenide and the molybdenum ions or a combination of both. By varying the MoS_2 amounts, CdSe-MoS_2 composites (**3**) with 0.1 to 48.0% of MoS_2 were synthesized. A Pt-CdSe composite (**4**) was obtained similarly by mixing dispersions of CdSe nanoribbons and citrate-stabilized Pt nanoparticles. The TEM shows the Pt particles as black dots of 5 ± 1 nm in diameter.

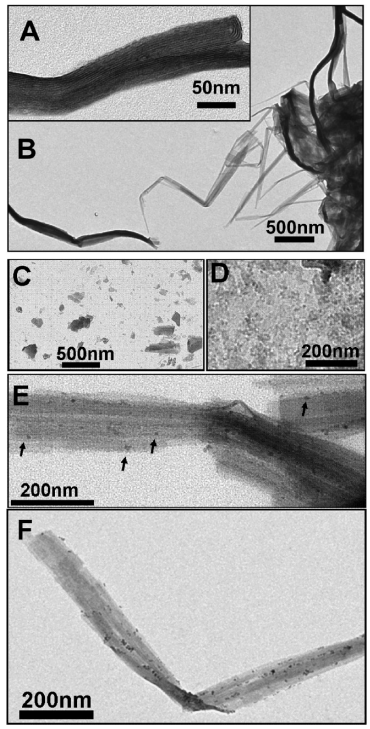

Figure 2. TEMs of precursors and composites. (A/B) CdSe nanoribbons at two magnifications. MoS_2 fragments directly after synthesis (C) and after 12 h of ultrasonication (D). (E) CdSe nanoribbons with 10% wt MoS_2 nanosheets attached (see arrows). (F) CdSe nanoribbon with 4% wt citrate-stabilized platinum nanoparticles (5 ± 1 nm).

The optical properties (Figure 3AB) of the composites (**3**) are mostly a sum of those of the separate components. The CdSe nanoribbons show their two distinctive absorption peaks at 421 and 452 nm, which correspond to the lowest energy excitations of this quantum well. The spectrum also shows a strong scattering contribution that is responsible for the tail reaching far into the visible region (450−800 nm). The MoS_2 nanoparticles cause a broad adsorption over the entire visible spectrum, which is due to multiple transitions in this small bandgap semiconductor (∼1 eV).[19] In **3**, the broad absorption of MoS_2 and the two distinctive peaks of the CdSe absorptions are combined. Fluorescence spectra (Figure 3B) of CdSe (**1**) and the CdSe-MoS_2 composite **3** (10% wt) are nearly identical; this suggests the extent of photochemical charge transfer from CdSe to MoS_2 is small.

Photocatalytic H_2 evolution experiments were conducted for 10 mg of each catalyst suspended in 100 mL of 0.1/0.1 M Na_2S/Na_2SO_3 solution, using light from a 300 W Xe lamp filtered through a 400 nm long-pass filter. The power density inside the flask was ∼450 mW/cm^2. Linear H_2 evolution (Figure 3C) is observed for CdSe nanoribbons (**1**), for all CdSe-MoS_2 composites (**3**), and for Pt-modified CdSe (**4**). Commercial CdSe powder was not active for the reaction. For **1** about 2.4 μmol of H_2 are evolved per hour. Using LED irradiation at 440 nm, a quantum yield of 9.2% was determined for **1**. That is a bit lower than our previously estimated value for broad spectral excitation ($\lambda = 400-800$ nm).[10] When Pt nanoparticles are loaded onto the nanoribbons, the activity remains unchanged. It is likely that the Pt surface becomes quickly coated with sulfide from the reaction mixture and selenide from the ribbons, hindering its ability to reduce protons. For bulk ZnS and CdS it has also been observed that Pt does not increase the photocatalytic activity.[1,9] This has been attributed to Pt promoting electron−hole recombination.

When 0.5% (mass) MoS_2 nanoparticles are loaded onto the CdSe nanoribbons, the activity increases to 8.9 μmol H_2/h, 3.7 times above the rate for **1**. But when the amount of MoS_2 is increased further, the activity diminishes again. The activity variation of **3** with MoS_2 loading is shown in Figure 3D. One can see a sharp initial increase followed by a sharp decrease and then a more shallow decrease beyond 2 mass percent of MoS_2. The two different regimes of diminishing activity suggest that there are at least two separate mechanisms for deactivation. The decrease at large loadings (>2% mass) is likely due to shading, that is, MoS_2 particles blocking light absorption by CdSe at 400−450 nm. This is supported by experiments with very large MoS_2 loading (48%, mass) where the activity falls below the value observed for pure nano-CdSe. Extrapolation to 100% loading leads to zero activity. The strong decrease of the activity at 1−2% loading, on the other hand, is likely due to other reasons. Probable are the blocking of active sites, perturbation of the electronic structure, and the introduction of recombination sites for electron hole pairs.

To further investigate the variation of the activity in compounds **1** and **3**, electrochemical and photoelectrochemical measurements were carried out on films of these materials that were deposited on gold foil as the working electrode. Photocurrent spectra for bulk CdSe, nano-CdSe (**1**), and CdSe-MoS_2 (**3**, 10%) are shown in Figure 4. In the presence of CH_3OH or Na_2S/Na_2SO_3 as sacrificial electron donors, all catalysts produce small photocurrents when the applied potential is sufficiently oxidizing. Photocurrents for nanomaterials are found to be almost ten times smaller (<5 μA/cm^2) than those measured for bulk CdSe film (<40 μA/cm^2). We attribute this to the absence of a space charge layer in the nanomaterials. In neutral methanol solution the photocurrent onsets occur at potentials ranging from −0.10 V for commercial CdSe to −0.55 V for nano-CdSe and −0.38 V for CdSe-MoS_2 (all NHE). When the semiconductors are biased at −1.15 V prior to the measurement and the scan is performed in the anodic direction (toward more oxidizing potentials), all photocurrent onsets are shifted by 200 mV to more negative values (data not shown), but the relative order of onset potentials within the series remains the same. We attribute the negative shift to a partial reduction of the semiconductor surface. Equating these potentials in Figure 4 with the conduction band edges[20−22] and using the optical bandgaps to calculate the valence band tops at E_{VB}, one can derive the energy scheme shown in Figure 5. It can be seen that the E_{CB} of nano-CdSe is by 0.45 V more reducing than E_{CB} of bulk CdSe and E_{CB} is 0.55 V more oxidizing. While nano-CdSe is able to reduce protons in neutral water, commercial CdSe is not. This enhanced flatband potential of nano-CdSe is a direct consequence of the quantum size effect, and it is the reason for the observed catalytic activity.

Figures 4 and 5 also show data from photocurrent measurements in 0.1/0.1 M Na_2S/Na_2SO_3 solution. In this electrolyte, we observe anodic photocurrents due to the oxidation of the sacrificial donors. When the applied bias is more negative than −0.4 to −0.5 V (NHE), a small cathodic current (<10 μA/cm^2) is also observed. The current is of similar magnitude for all tested samples and only occurs in the presence of sulfide or sulfite as an electrolyte. Thus, we do not attribute it to the CdSe samples, but to the formation of photoactive metal sulfides on the gold electrode. The cathodic photocurrent shall be neglected in the following discussion. Onset potentials for anodic photocurrents are observed in the small interval of −0.41 to −0.49 V, close to the redox potential of the sulfur/hydrosulfide couple ($E^\circ = -0.48$ V, NHE). We attribute this to a Fermi level

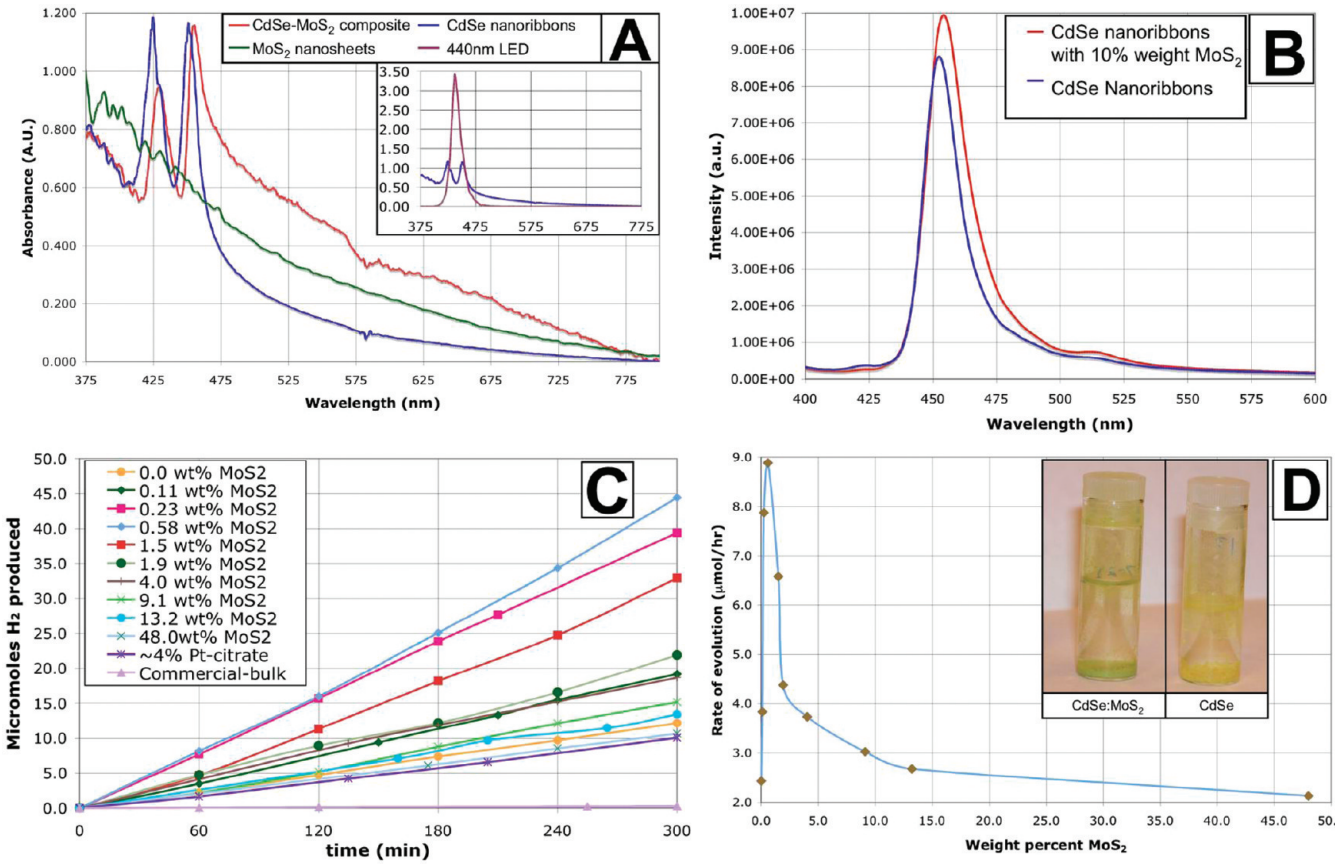

Figure 3. (A) UV−vis spectra (feature at 575 nm is an artifact from the deuterium lamp). (B) Fluorescence spectra in water (λ_{ex} = 375 nm). (C) H_2 evolution with time. (D) Variation of initial H_2 evolution activity with MoS_2 loading (mass %). Insert: photos of nano-CdSe-MoS_2 and nano-CdSe.

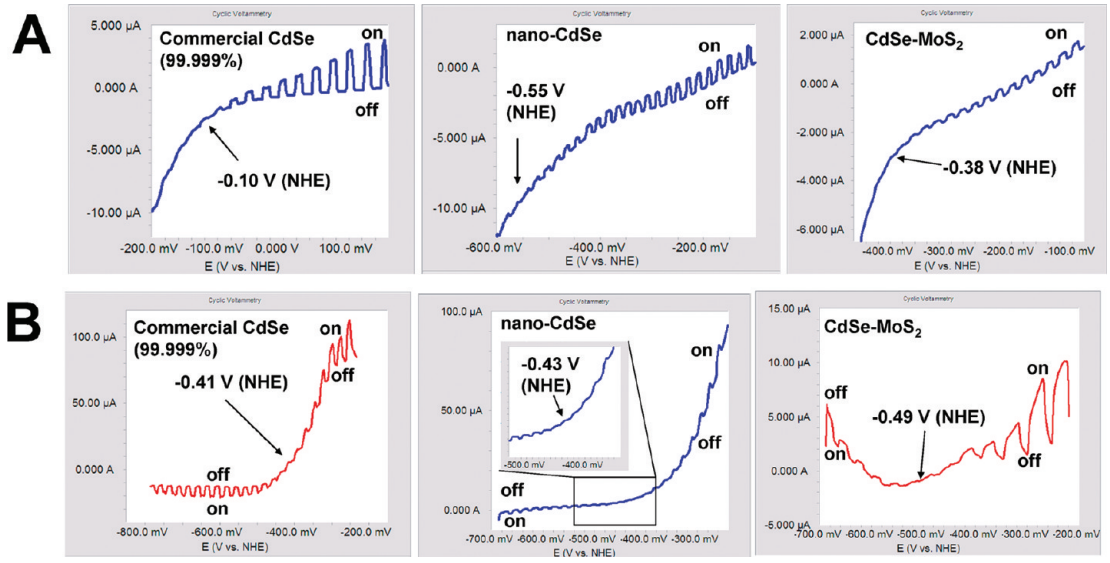

Figure 4. Photocurrent spectra (chopped light) in (A) 1.0 M aqueous KCl solution containing 20% (v/v) methanol and (B) in 0.1 M Na_2S/0.1 M Na_2SO_3 solution (pH = 9.3). Scan speed = 10 mV/s, scan direction = cathodic (right to left).

equilibration between semiconductors and the HS^-/S_2^{2-} redox couple in solution. For bulk CdSe, hydrosulfide has been known to shift the flatband potential by −0.3 V,[23] exactly as observed here. The opposite effect is achieved with nano-CdSe. Here hydrosulfide reduces the flatband potential by ∼+100 mV. We presently do not know if this shift proceeds via adsorption of the hydrosulfide to the semiconductor surface or not. We note, however, that nano-CdSe irradiated in hydrosulfide solution shows optical characteristics of a CdS coating.[10] On the basis of the flatband potential in sulfide solution, bulk CdSe should also be able to reduce protons in hydrosulfide solution, but this is not observed. It seems that hydrosulfide binding leads to a CdSe@CdS core shell system,[24] which confines photogenerated holes to the core and renders them inactive for SH^- oxidation.

To obtain more insight into the mechanism by which MoS_2 activates nano-CdSe, additional cyclic voltammograms were recorded in 0.1/0.1 M Na_2S/Na_2SO_3 (Figure 6A).

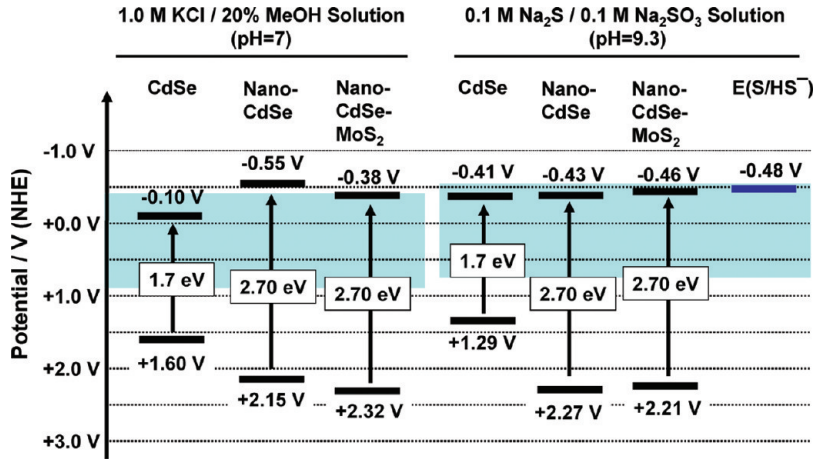

Figure 5. Band edge potentials obtained from photocurrent onset potentials in Figure 4. The proton reduction potential (−0.41 V) and the water oxidation potential (+0.82 V) at neutral pH are shown by the borders of the gray band. In sulfite/sulfide solution these values are −0.55 V and +0.68 V, respectively, due to the increase in pH to 9.3.

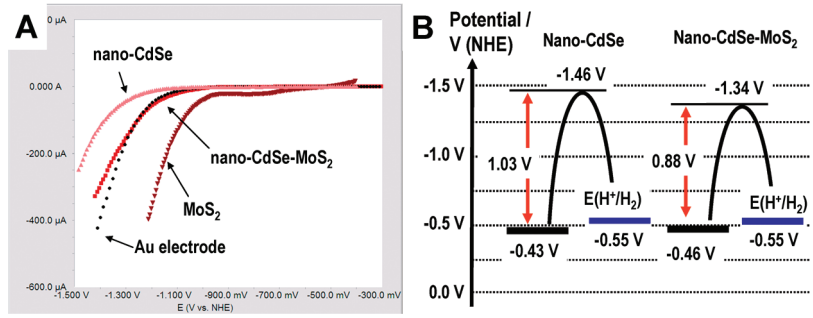

Figure 6. (A) Cyclic voltammograms in 0.1/0.1 M Na_2S/Na_2SO_3 solution (pH = 9.3). HER evolution potentials at 200 $\mu A/cm^2$ were as follows: nano-CdSe, $E = -1.46$ V; nano-CdSe-MoS_2, $E = -1.34$ V; MoS_2, $E = -1.14$ V; Au, $E = -1.32$ V. (B) Band energy diagram for nano-CdSe and CdSe-MoS_2 in 0.1 M Na_2S/0.1 M Na_2SO_3 solution (pH = 9.3), showing activation barriers for proton reduction.

The plots reveal cathodic currents due to the reduction of protons at potentials below ∼−1.0 V (NHE). Molybdenum disulfide nanoparticles are found to reduce protons at −1.14 V (200 $\mu A/cm^2$), approximately 0.7 V more negative than the thermodynamic value. This overpotential is less favorable than what has been observed by Bonde et al., who obtain −0.3 V (at pH = 0.4, this equals ∼−0.7 V at pH = 7) for the proton reduction potential of a MoS_2 film.[25] We attribute the lesser activity of our MoS_2 to partial air oxidation of the nanoparticles during preparation and workup. Edge site oxidation is the predominant mechanism for MoS_2 inactivation.[25] The data in Figure 6A reveal a very negative proton reduction potential (−1.46 V) for nano-CdSe, which can be raised to −1.34 V after the attachment of 10% (mass) MoS_2 nanoparticles. Thus, the increased activity of the nano-CdSe-MoS_2 photocatalyst can be attributed to lowering of the H^+ reduction overpotential.

Using the measured proton reduction potentials and the conduction band edges for nano-CdSe and CdSe-MoS_2, we have constructed an energy scheme for proton reduction in sulfite/sulfide solution (Figure 6B). One can see that, in this electrolyte, the conduction band edges of both catalysts remain ∼100 mV below the proton reduction potential (−0.55 V at pH = 9.3). This is probably the reason for the low observed quantum efficiency of 9.2% at 440 nm. Nevertheless, the process can go forward because the substantial activation barrier for the electrochemical H^+/H_2 conversion slows down the backreaction. The activation energies for HER are 0.88 and 1.03 eV, with the smaller value for the more active CdSe-MoS_2. These values reflect mainly the electrochemical overpotentials and a barrier for electron transport from CdSe to MoS_2. Considering that the individual MoS_2 nanoparticles have a H^+ reduction overpotential of 0.7 V, the barrier for electron transport can then be estimated as ∼0.18 V (= 0.88 V − 0.7 V) per transferred electron. These results suggest that further catalyst optimization should be possible by either replacing MoS_2 with a more effective HER catalyst or by replacing nano-CdSe with a semiconductor that has a more reducing conduction band edge.

Conclusions

In summary we have shown that CdSe-MoS_2 and CdSe-Pt nanocomposites can be constructed in the solution phase from separate nanoscale building blocks.

Platinum is not effective as cocatalyst, which is likely due to sulfide poisoning of surface sites. MoS_2 nanoparticles obtained by chemical exfoliation are effective cocatalysts for H_2 evolution, enhancing the activity of nano-CdSe by up to 3.7 times. Electrochemical measurements reveal that MoS_2 activates the photocatalyst by lowering the electrochemical proton reduction overpotential. However, when the concentration of MoS_2 is increased, deactivation of the photocatalyst takes place due to MoS_2 absorbing some of the photons (shading). A strong decay of activity at small MoS_2 loadings suggests that an additional but yet unknown mechanism exists for deactivation. Most likely is that the treatment with MoS_2 nanoparticles introduces recombination sites for photogenerated electron hole pairs. The photoelectrochemical data proves that the activation of nano-CdSe is due to a quantum size effect that raises the flatband potential to −0.55 V compared to bulk CdSe (−0.10 V). In sulfite/sulfide solution flatband potentials of both semiconductors

are fixed by SH^- potential determining ions. In the case of bulk CdSe, the coating with SH^- produces a CdSe@CdS core shell system that remains inactive for the photocatalytic HER, presumably because it confines photogenerated electrons to the CdSe core.

Acknowledgment. This work was supported by Grant # 0829142 of the National Science Foundation.

References and Notes

(1) Buhler, N.; Meier, K.; Reber, J. F. *J. Phys. Chem.* **1984**, *88* (15), 3261–3268.
(2) Tsuji, I.; Kato, H.; Kudo, A. *Chem. Mater.* **2006**, *18* (7), 1969–1975.
(3) Tsuji, I.; Kato, H.; Kobayashi, H.; Kudo, A. *J. Am. Chem. Soc.* **2004**, *126* (41), 13406–13413.
(4) Zheng, N.; Bu, X. H.; Vu, H.; Feng, P. Y. *Angew. Chem., Int. Ed. Engl.* **2005**, *44* (33), 5299–5303.
(5) Zheng, N. F.; Bu, X. H.; Feng, P. Y. *J. Am. Chem. Soc.* **2005**, *127* (15), 5286–5287.
(6) Lei, Z. B.; Ma, G. J.; Liu, M. Y.; You, W. S.; Yan, H. J.; Wu, G. P.; Takata, T.; Hara, M.; Domen, K.; Li, C. *J. Catal.* **2006**, *237* (2), 322–329.
(7) Bessekhouad, Y.; Mohammedi, M.; Trari, M. *Sol. Energy Mater. Sol. Cells* **2002**, *73* (3), 339–350.
(8) Sobczynski, A.; Yildiz, A.; Bard, A. J.; Campion, A.; Fox, M. A.; Mallouk, T.; Webber, S. E.; White, J. M. *J. Phys. Chem.* **1988**, *92* (8), 2311–2315.
(9) Reber, J. F.; Meier, K. *J. Phys. Chem.* **1984**, *88* (24), 5903–5913.
(10) Frame, F. A.; Carroll, E. C.; Larsen, D. S.; Sarahan, M. S.; Browning, N. D.; Osterloh, F. E. *Chem. Commun.* **2008**, 2206–2208.
(11) Nielsen, J. H.; Bech, L.; Nielsen, K.; Tison, Y.; Jorgensen, K. P.; Bonde, J. L.; Horch, S.; Jaramillo, T. F.; Chorkendorff, I. *Surf. Sci.* **2009**, *603* (9), 1182–1189.
(12) Zong, X.; Na, Y.; Wen, F. Y.; Ma, G. J.; Yang, J. H.; Wang, D. G.; Ma, Y.; Wang, M.; Sun, L.; Li, C. *Chem. Commun.* **2009**, (30), 4536–4538.
(13) Zong, X.; Yan, H. J.; Wu, G. P.; Ma, G. J.; Wen, F. Y.; Wang, L.; Li, C. *J. Am. Chem. Soc.* **2008**, *130* (23), 7176+.
(14) Hinnemann, B.; Moses, P. G.; Bonde, J.; Jorgensen, K. P.; Nielsen, J. H.; Horch, S.; Chorkendorff, I.; Norskov, J. K. *J. Am. Chem. Soc.* **2005**, *127* (15), 5308–5309.
(15) Jaramillo, T. F.; Jorgensen, K. P.; Bonde, J.; Nielsen, J. H.; Horch, S.; Chorkendorff, I. *Science* **2007**, *317* (5834), 100–102.
(16) Joo, J.; Son, J. S.; Kwon, S. G.; Yu, J. H.; Hyeon, T. *J. Am. Chem. Soc.* **2006**, *128* (17), 5632–5633.
(17) Joensen, P.; Frindt, R. F.; Morrison, S. R. *Mater. Res. Bull.* **1986**, *21* (4), 457–461.
(18) Harriman, A.; Millward, G. R.; Neta, P.; Richoux, M. C.; Thomas, J. M. *J. Phys. Chem.* **1988**, *92* (5), 1286–1290.
(19) Yoffe, A. D. *Chem. Soc. Rev.* **1976**, *5* (1), 51–78.
(20) Bard, A. J.; Faulkner, L. R. *Electrochemical methods: fundamentals and applications*, 2nd ed.; John Wiley: New York, 2001; p 754.
(21) Ishikawa, A.; Takata, T.; Kondo, J. N.; Hara, M.; Kobayashi, H.; Domen, K. *J. Am. Chem. Soc.* **2002**, *124* (45), 13547–13553.
(22) Akatsuka, K.; Takanashi, G.; Ebina, Y.; Sakai, N.; Haga, M.; Sasaki, T. *J. Phys. Chem. Solids* **2008**, *69* (5−6), 1288–1291.
(23) Frese, K. W.; Canfield, D. G. *J. Electrochem. Soc.* **1984**, *131* (11), 2614–2618.
(24) Peng, X. G.; Schlamp, M. C.; Kadavanich, A. V.; Alivisatos, A. P. *J. Am. Chem. Soc.* **1997**, *119* (30), 7019–7029.
(25) Bonde, J.; Moses, P. G.; Jaramillo, T. F.; Norskov, J. K.; Chorkendorff, I. *Faraday Discuss.* **2008**, *140*, 219–231.

JP101308E